Vaporization and Melting of Materials in Fusion Devices

A.M. Hassanein, G.L. Kulcinski, and W.G. Wolfer

August 1981

UWFDM-422

Paper presented at Second Topical Mtg. on Fusion Reactor Materials, August 9-12, 1981, Seattle WA; J. Nucl. Matls. 103 & 104, 321-326 (1981).

FUSION TECHNOLOGY INSTITUTE

UNIVERSITY OF WISCONSIN

MADISON WISCONSIN

Vaporization and Melting of Materials in Fusion Devices

A.M. Hassanein, G.L. Kulcinski, and W.G. Wolfer

Fusion Technology Institute
University of Wisconsin
1500 Engineering Drive
Madison, WI 53706

http://fti.neep.wisc.edu

August 1981

UWFDM-422

Paper presented at Second Topical Mtg. on Fusion Reactor Materials, August 9-12, 1981, Seattle WA; J. Nucl. Matls. 103 & 104, 321-326 (1981).

Vaporization and Melting of Materials in Fusion Devices

A. M. Hassanein

G. L. Kulcinski

W. G. Wolfer

Fusion Engineering Program
Nuclear Engineering Department
University of Wisconsin
Madison, WI 53706

August 1981

UWFDM-422

VAPORIZATION AND MELTING OF MATERIALS IN FUSION DEVICES

A. M. Hassanein, G. L. Kulcinski, and W. G. Wolfer

Fusion Engineering Program, Nuclear Engineering Department
University of Wisconsin, Madison, WI 53706, USA

High energy fluxes on first wall materials and other components are encountered in magnetic fusion devices, particularly during hard plasma disruptions. A model to predict evaporation and melting is described which contains a formulation of the evaporation kinetics based on transport theory results. The effect of vapor shielding is evaluated under the assumption that plasma ions slowed down in the vapor dissipate their energy in an isotropic manner. Specific results on melting and evaporation are given for 316 SS, Mo, and graphite.

1. INTRODUCTION

Intense heat fluxes on limiters, the plasma chamber wall, on divertor plates, and neutral beam dumps will be encountered in magnetic fusion devices. Of particular concern are unipolar arcing, run-away electrons striking the limiter, and plasma dump following a hard disruption. The energy deposited on part of the first wall during a plasma disruption in the next generation of fusion devices such as FED and INTOR is of the order of 300 MJ, and the deposition time is estimated to be between 1 ms and 100 ms. As a result, the energy or heat flux may reach values from 10 to 1000 kW/cm^2. Melting and evaporation of first wall and limiter materials may then occur.

It is therefore important to evaluate the amount of material evaporated from the exposed material surfaces for two reasons. First, the evaporated atoms may contaminate the plasma with high-Z material. Second, both evaporation and melting will contribute to the first wall erosion in addition to erosion from sputtering if plasma disruptions occur repeatedly.

Previous estimates of the evaporation of first wall materials were based on models valid either for slow or intense evaporation. The former has been developed by Behrisch [1,2], and it is based on the assumption that the energy expended in both melting and evaporation is negligible compared to the energy conducted into the material. Therefore, one simply solves a heat conduction problem with a fixed surface boundary. The time-dependent surface temperature so obtained is used to compute the evaporation rate into a vacuum according to the vapor pressure relationship.

A model for intense evaporation as developed by Andrews and Atthey [3] was applied recently [4] to plasma disruptions. Here, it is assumed that, after a preheat time, evaporation begins when the surface temperature reaches the boiling point of the liquid metal determined by the ambient vapor pressure. Unfortunately, no clear definition of an ambient vapor pressure can be given for the low pressures existing in a magnetic fusion plasma chamber.

In fact, the surface temperature is determined by both the boundary condition as well as by the kinetics of the evaporation process. The correct boundary condition entails partitioning of the incident energy flux into conduction, melting, evaporation, and radiation. Consequently, the heat conduction problem is one involving two moving boundaries, one being the melt-solid interface, and the other the surface receding as a result of evaporation.

The kinetics of evaporation establish the connection between the surface temperature and the net atom flux leaving the surface taking into account the possibility of recondensation.

A model containing all these features has been developed and will be described briefly in sections 2, 3, and 4. A more extensive and detailed description will be published elsewhere. A related approach has recently been developed by Merrill [5]. However, our model differs substantially with regard to the kinetics of the evaporation process and it also includes vapor shielding. Results obtained with our model will be given in section 5 for stainless steel, molybdenum, and graphite. The implication of these results in the first wall design of future fusion devices will be presented in section 6.

2. HEAT CONDUCTION WITH MELTING AND EVAPORATION

If we assume a uniform energy flux strikes part of the first wall, the heat conduction can be considered to be one-dimensional.

For time periods less than t_m (the time to reach the melting point on the surface), the heat conduction equation,

$$\rho_s C_s \frac{\partial T_s}{\partial t} - \nabla \cdot K_s \nabla T_s = 0 \qquad (1)$$

must be solved subject to the boundary conditions that $T = T_o$ = constant on the coolant

side, and

$$F(t) = -K_s \frac{\partial T_s}{\partial x} + \rho_s(T_v)L_v v(t) + \sigma(T_v^4 - T_o^4) \quad (2)$$

on the surface facing the plasma. Here F(t) is the heat flux, $\rho_s(T)$ is the density, $C_s(T)$ the specific heat, $K_s(T)$ the thermal conductivity of the solid material. The heat of vaporization is L_v; T_s is the temperature in the solid; T_v is the surface temperature; and v(t) is the velocity of the receding surface. The velocity stated simply as v(t) in Eq. (2) is a function of the instantaneous surface temperature and other material parameters and might be more properly written as $v(T_v(t))$. Furthermore, the radiative heat transfer term contains the Stefan-Boltzmann constant σ and the surface temperature T_o of the cold portion of the first wall. The second term in Eq. (2), which will be discussed shortly in connection with the evaporation energy loss rate, is negligible for temperatures below the melting point.

Once melting occurs, the condensed phase consists of two regions:

a) $s(t) < x < m(t)$ for the melt layer

b) $m(t) < x$ for the solid phase.

where: s(t) is the instantaneous distance of the melted surface,
m(t) is the distance of the melted layer from the surface.

Equation (1) applies again to the solid phase, but the boundary conditions are now that at x = m(t)

$$T_s(m(t),t) = T_\ell(m(t),t) = T_m \quad (3a)$$

and

$$-K_\ell \frac{\partial T_\ell}{\partial x}\Big|_{m(t)} = -K_s \frac{\partial T_s}{\partial x}\Big|_{m(t)} + \rho_s L_f w(t) \quad (3b)$$

where T_m is the melting temperature, T_ℓ is the temperature in the melt layer, L_f the latent heat of fusion, and

$$w(t) = \frac{dm}{dt} \quad (4)$$

is the velocity of the melt-solid interface. In the melt layer, the heat conduction equation is

$$\rho_\ell C_\ell \frac{\partial T_\ell}{\partial t} - \nabla \cdot K_\ell \nabla T_\ell = 0 \quad . \quad (5)$$

The solution in the melt layer must satisfy the boundary conditions (3) and (4) on x = m(t) and the condition

$$F(t) = -K_\ell \frac{\partial T_\ell}{\partial x}\Big|_{s(t)} + \rho_\ell(T_v)L_v v(t) + \sigma(T_v^4 - T_o^4) \quad (6)$$

on the surface x = s(t).

The solution of these equations in a coordinate frame moving with the receding surface is contained in the computer code A*THERMAL [6]. A more detailed description of the solution methods and the formulation of the problem in the moving frame will be given elsewhere.

In order to achieve high accuracy for the surface temperature and for the advance of the melt-solid interface, variable thickness zones are used. The spacing of the grid points is chosen to be small near the surface, and increases with increasing depth into the material.

3. KINETICS OF EVAPORATION

The net flux of atoms leaving the surface may be considered to consist of two parts according to the equation

$$J = J_e^{eq}(T_v) - J_c(T_c) \quad (7)$$

where the first term represents the vacuum evaporation flux

$$J_e^{eq}(T_v) = (2\pi m k T_v)^{-1/2} \sigma_e P_s(T_v) \quad (8)$$

and $J_c(T_c)$ the recondensation flux of the vapor with a temperature T_c. Here, m is the mass of the vapor species, σ_e the evaporation coefficient, and

$$P_s = P_o \exp(-\Delta H/kT) \quad (9)$$

is the saturation vapor pressure of the material characterized by the pre-exponential factor P_o and the activation energy for evaporation, ΔH.

As the material begins to vaporize, the vapor expands at first freely into the vacuum. Initially, the net evaporation flux leaving the surface is therefore equal to J_e^{eq}, but it decreases thereafter due to recondensation. This process of recondensation arises from two facts. First, the density of vapor expanding into a vacuum retains a finite value for t > 0 in front of the surface. Second, atoms evaporated subsequently from the surface may collide with the already present vapor phase and be backscattered towards the surface where they may be

reabsorbed. The fraction of recondensing atoms will increase as the vapor density and the spatial extension of the vapor phase increases with time. However, an asymptotic value of about 0.2 is reached for this fraction after about 20 collision times according to the transport calculations by Anisimov and Rakhmatulina [7]. The collision time τ_c for the vapor atoms is given by

$$\frac{1}{\tau_c} = 16\sqrt{\pi}\, na^2\, (kT_v/m)^{1/2} \qquad (10)$$

where πa^2 is the elastic scattering cross section for the vapor atoms and n the vapor density in front of the surface. The latter can be related to the maximum vacuum evaporation rate according to

$$J_e^{eq} = \frac{1}{4}\,\bar{v}n = n(kT_v/2\pi m)^{1/2} \qquad (11)$$

where we used the relation

$$\bar{v} = (8kT_v/\pi m)^{1/2}$$

for the average velocity of the vapor species.

For the elastic scattering cross section we may use the approximation that

$$\frac{4\pi}{3}\, a^3 = \Omega$$

where Ω is the molecular volume. Then, the collision time τ_c is given by

$$\frac{1}{\tau_c} = 16\sqrt{2}\,\pi^{1/3}\,(\tfrac{3}{4}\,\Omega)^{2/3}\, J_e^{eq} \quad . \qquad (12)$$

According to the numerical results of Anisimov and Rakhmatulina [7], the recondensation flux may be approximated by

$$J_c = 0.2\, J_e^{eq}\,[1 - \exp\,(-t/\tau_R)] \qquad (13)$$

so that the net flux is given by

$$J(t) = J_e^{eq}\,[0.8 + 0.2\exp\,(-t/\tau_R)] \quad . \qquad (14)$$

The relaxation time τ_R to reach, say, 98% of the full amount of recondensation after 20 collision times τ_c, is given by

$$\tau_R = 20\,\tau_c/\ell n\ 10 \cong 10\,\tau_c$$

or

$$\frac{1}{\tau_R} = 1.6\sqrt{2}\,\pi^{1/3}\,(\tfrac{3}{4}\,\Omega)^{2/3}\, J_e^{eq} \quad . \qquad (15)$$

Finally, we note that the velocity of the receding surface is given by

$$v(t) = \Omega J(t) \quad . \qquad (16)$$

4. VAPOR SHIELDING

The heat flux F(t) on the first wall during a disruption consists to a large part of the plasma ions. It is generally believed that a sheath potential of the order of 10 kV exists at the onset of the plasma disruption. The plasma ions will therefore strike the first wall with a kinetic energy of about 10 keV. The average range of the plasma ions in a stainless steel wall is about 7.5×10^{-8} m. Because of this short range, it is indeed appropriate to treat the energy deposition as a surface heat flux rather than a volumetric heat deposition.

On the other hand, if a vapor layer of sufficient thickness has been produced, the plasma ions will be stopped in this vapor layer rather than in the condensed material of the first wall. The vapor layer, in the process of stopping the plasma ions, will be partially ionized, excited, and heated. Subsequently, the energy stored in this vapor layer will be emitted in the form of X-rays, optical radiation, and thermal diffusion of the hot vapor atoms. As a result, the energy flux of the plasma particles is converted from a unidirectional one into a more isotropic one. If we assume in fact that the converted energy flux has become isotropic, only one half of the original, unidirectional energy flux will now strike the part of the first wall exposed to the plasma disruption.

Accordingly, we have modeled the effect of vapor shielding in the following manner. If F_o is the magnitude of the initial energy flux, and R the range of plasma ions in the condensed phase of the first wall, a vapor layer produced by the evaporation of a thickness $\Delta x(t) < R$ will reduce the surface heat flux to the first wall to the value of

$$F(t) = F_o\,[1 - \Delta x(t)/R] + \tfrac{1}{2}\,F_o\Delta x(t)/R$$
$$= F_o\,[1 - \Delta x(t)/2R] \quad . \qquad (16)$$

When the evaporation thickness $\Delta x(t) > R$, then

$$F(t) = \tfrac{1}{2}\,F_o \quad . \qquad (17)$$

The present model for vapor shielding assumes

that the atoms will not be transported preferentially parallel to the surface. The slowing-down of plasma ions in the vapor implies, of course, that some ionization will occur. It is therefore possible that the ionized vapor will be removed in a lateral direction parallel to the field lines, so that the vapor density in front of the exposed surface is reduced. Since little is known about such a transport mechanism, all calculations were done with and without vapor shielding.

5. RESULTS

The estimated deposition times for plasma disruption vary widely, but it is generally agreed that they are on the order of or less than 100 ms. Longer deposition times result in lower surface temperatures than shorter times. Accordingly, the present calculations were carried out for shorter deposition times equal to 5, 10, and 20 ms, and for energy densities as large as 1300 J/cm^2. Furthermore, it was assumed that the energy is deposited at a constant rate F_o over the assumed disruption time.

Figures 1 and 2 show the maximum thickness of the melt layer for stainless steel without and with vapor shielding, respectively. The thermophysical properties are those given in Ref. [8], and the initial temprature was assumed to be T_o = 573°K. It is seen that melting requires a minimum or threshold energy density flux. With increasing energy density, the melt layer thickness rises rapidly, reaches a maximum, and then declines somewhat. The existence of a maximum is explained by the fact that vaporization is a highly nonlinear function of temperature. As the energy flux goes up, the evaporation rate increases exponentially, consuming an ever larger fraction of the deposited energy. Eventually, however, the evaporation rate will reach a saturation level at energy fluxes higher than considered here. In this case, the melt thickness is also expected to reach a constant value, and the surface and melt interface recede at the same rate. Figure 3 shows the thickness of the evaporated layer for 1000 disruptions. Whereas vapor shielding had only a minor effect on the melt layer thickness, it affects the evaporation by at least an order of magnitude. The insensitivity of the melt layer thickness to vapor shielding is due to the fact that melting of stainless steel precedes evaporation by a relatively large time interval. This is expected for all metals with a relatively low melting point. Conversely, refractory metals with high melting points are expected to benefit from vapor shielding with regard to both melting and evaporation. The results for molybdenum shown in Figs. 4, 5, and 6 confirm this point. These results were obtained with the thermophysical properties given in Refs. [9,10] and for an initial temperature of T_o = 573°K. Mo, as compared to stainless steel, requires a higher threshold energy density for melting to occur. Furthermore, the evaporation is substantially less than for stainless steels.

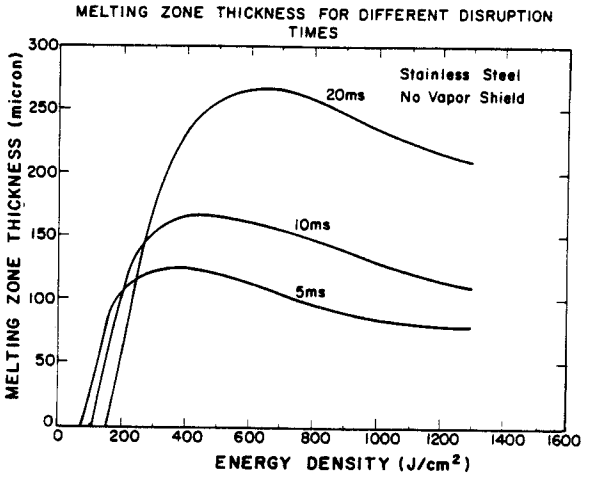

Figure 1. Stainless steel melting zone thickness with no vapor shield as a function of energy density.

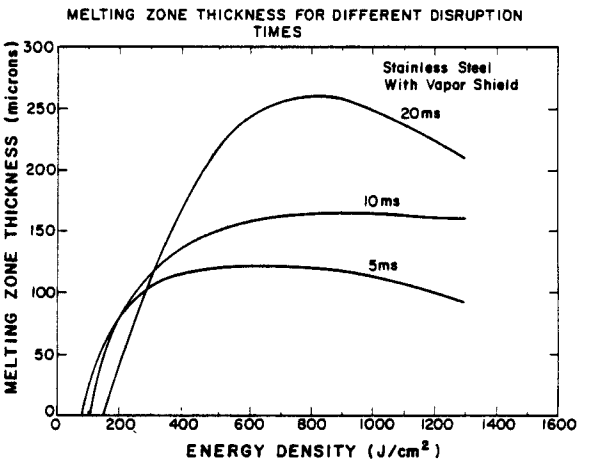

Figure 2. Stainless steel melting zone thickness with vapor shield as a function of energy density.

However, since Mo has a higher atomic number, small amounts of Mo impurities are detrimental to plasma stability. For this reason, Fig. 6 shows the evaporation thickness down to 10^{-6} cm per 1000 plasma disruptions, even though these low values are of little concern to the structural integrity of a component made of Mo.

Graphite has been considered as a suitable material for both limiters and first wall protection. In its latter capacity, it is expected that the surface temperature is high before a plasma disruption. Hence, the calculations for graphite were carried out with T_o = 1500 K; the

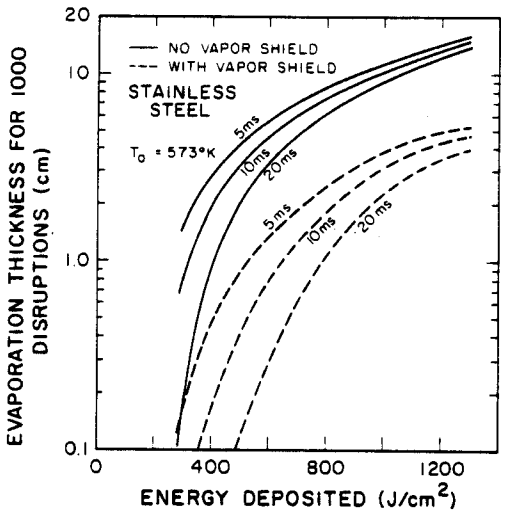

Figure 3. Evaporation thickness of stainless steel for 1000 disruptions for different energy deposited.

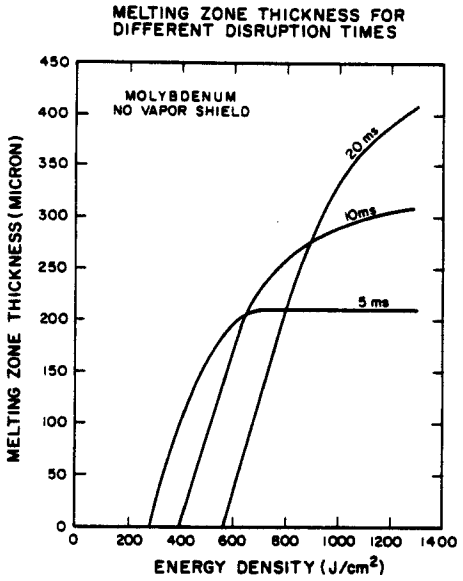

Figure 4. Molybdenum melting zone thickness with no vapor shield as a function of energy density.

thermophysical properties are those given in Ref. [11]. The results for the evaporation thickness shown in Fig. 7 were obtained assuming that the vapor species is monatomic carbon. It is however known that in the saturated vapor of graphite at T = 2733, the trimer population is higher by a factor of 9 than the monomer population [12]. Therefore, if we were to assume that the dominant vapor species is C_3 rather than monatomic carbon, then the evaporation thicknesses in Fig. 7 would have to be increased by a factor of $\sqrt{3}$.

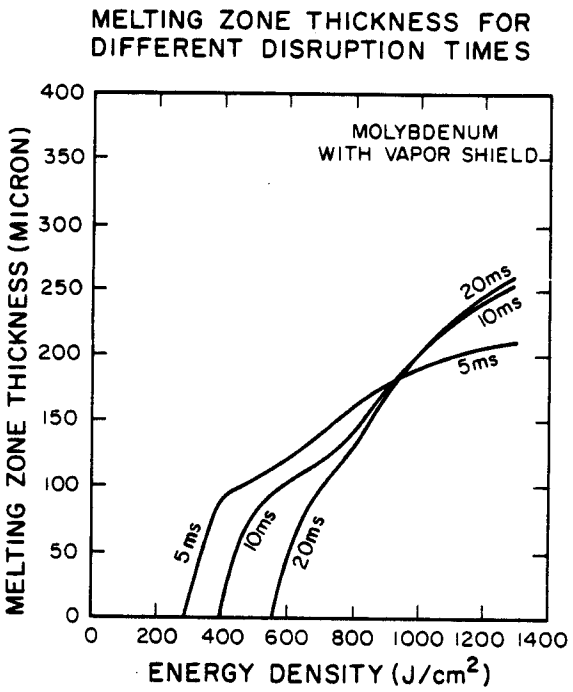

Figure 5. Molybdenum melting zone thickness with vapor shield for different energy deposited.

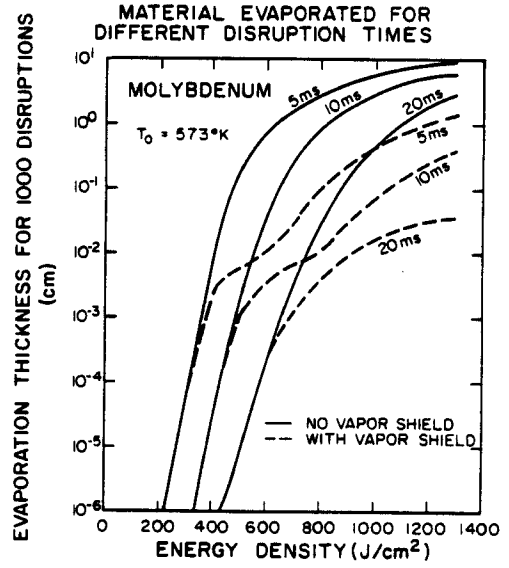

Figure 6. Evaporation thickness of molybdenum for 1000 disruptions as a function of energy density.

6. CONCLUSIONS

A model and computer code have been developed to solve the heat conduction problem with phase

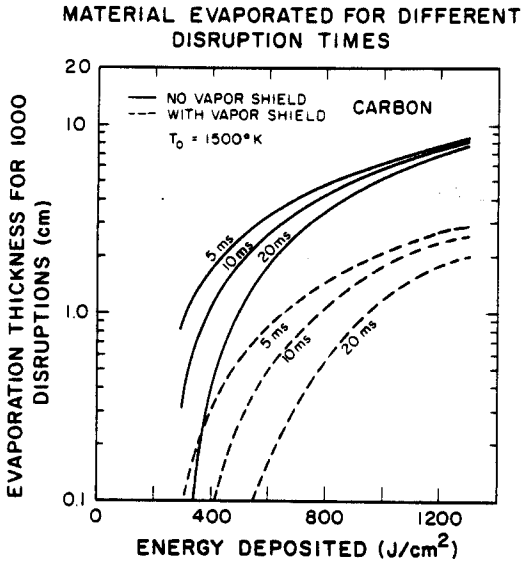

Figure 7. Evaporation thickness of carbon for 1000 disruptions as a function of energy density.

changes and two moving boundaries, one for the melt-solid interface, and one for the evaporating surface. This model has been applied to study melting and evaporation during plasma disruptions. Results are shown for 316 stainless steel, Mo, and graphite as first wall materials. Comparing our results to those earlier reported [1,2,4,5] we reach the following conclusions:

a) The energy expended in both melting and evaporation cannot be neglected in the solution of the heat conduction problem.

b) The temperature dependence of all thermophysical properties for both solid and liquid phase must be included in the model.

c) The net evaporation flux reduces with time and approaches 80% of the vacuum evaporation flux after 20 collision times in the vapor phase.

d) Vapor shielding, i.e., the stopping of plasma ions by the vapor leads to a significant reduction of the material evaporated in a disruption.

e) The melt layer thickness is affected by vapor shielding only for materials with high melting points.

f) Significant melting or evaporation occurs only above a characteristic energy density. This threshold depends both on the material and the rate of energy deposition.

ACKNOWLEDGEMENT

The authors would like to acknowledge the partial support by the Japanese Atomic Energy Research Institute (JAERI) and the Wisconsin Electric Utilities Research Foundation (WEURF) for this work.

REFERENCES

[1] Behrisch, R., Nucl. Fusion 12 (1972) 695.

[2] Behrisch, R., J. Nucl. Matls. 93 & 94 (1980) 498.

[3] Andrews, J.G. and Atthey, D.R., J. Inst. Maths Applics. 15 (1975) 59.

[4] Loebel, L.L. and Wolfer, W.G., Evaporation under intense energy deposition, UWFDM-370, University of Wisconsin, Aug. 1980.

[5] Merrill, B., Contribution to US INTOR Report INTOR/NUC/81-7, June 1981.

[6] Hassanein, A.M. and Kulcinski, G.L., A*THERMAL computer code description, to be published.

[7] Anisimov, S.I. and Rakhmatulina, A.Kh., Sov. Phys. JETP 37 (1973) 441.

[8] Choong, S. Kim, Thermophysical properties of stainless steels, ANL-75-55, Argonne National Laboratory, September 1975.

[9] Betz, G. and Frohberg, M.G., Enthalpy measurements on solid and liquid molybdenum by levitation calorimetry, High Temperature-High Pressures 12 (1980) 169-178.

[10] Seydel, U., Bauhof, H., Fucke, W., and Wadle, H., Thermophysical data for various transition metals at high temperatures obtained by submicrosecond-pulse-heating methods, High Temperatures-High Pressures 11 (1979) 635-642.

[11] Rasor, N.S. and McClelland, J.D., Thermal properties of graphite, molybdenum and tantalum to their destruction temperatures, J. Phys. Chem. Solids 15 (1959) 17-26.

[12] Gingerich, K.A., Cocke, D.L., and Kingcade, J.E., Inorg. Chimica Acta 17 (1976) L1.